Journal of Power Sources 270 (2014) 554–563

Contents lists available at ScienceDirect

Journal of Power Sources

journal homepage: www.elsevier.com/locate/jpowsour

Hydrogen storage systems from waste Mg alloys

C. Pistidda [a, *], N. Bergemann [a], J. Wurr [a], A. Rzeszutek [a], K.T. Møller [b], B.R.S. Hansen [b], S. Garroni [c], C. Horstmann [a], C. Milanese [d], A. Girella [d], O. Metz [a], K. Taube [a], T.R. Jensen [b], D. Thomas [e], H.P. Liermann [f], T. Klassen [a], M. Dornheim [a]

[a] Institute of Materials Research, Materials Technology, Helmholtz-Zentrum Geesthacht GmbH, Max-Planck-Strasse 1, D-21502 Geesthacht, Schleswig-Holstein, Germany
[b] Center for Materials Crystallography, iNANO, and Department of Chemistry, Aarhus University, Langelandsgade 140, 8000 Aarhus, Denmark
[c] Dipartimento di Chimica e Farmacia, Università di Sassari and INSTM, Via Vienna 2, I-07100 Sassari, Italy
[d] Pavia H_2 Lab, C.S.G.I. & Dipartimento di Chimica, Sezione di Chimica Fisica, Università di Pavia, Viale Taramelli 16, Pavia I-27100, Italy
[e] MAX IV Laboratory, Lund University, Römers väg 1, 22363 Lund, Sweden
[f] Photon Science, Deutsches Elektronen Synchrontron DESY, Hamburg, Germany

HIGHLIGHTS

- Mg based wastes can be used for H_2 storage purposes.
- The hydrogenated alloys show a H_2 capacity of ~6 wt.%.
- The conversion process is possible and easily achievable.

ARTICLE INFO

Article history:
Received 11 April 2014
Received in revised form
11 July 2014
Accepted 21 July 2014
Available online 30 July 2014

Keywords:
Hydrogen storage
Magnesium waste
Hydrogen storage
Magnesium waste

ABSTRACT

The production cost of materials for hydrogen storage is one of the major issues to be addressed in order to consider them suitable for large scale applications. In the last decades several authors reported on the hydrogen sorption properties of Mg and Mg-based systems. In this work magnesium industrial wastes of AZ91 alloy and Mg-10 wt.% Gd alloy are used for the production of hydrogen storage materials. The hydrogen sorption properties of the alloys were investigated by means of volumetric technique, *in situ* synchrotron radiation powder X-ray diffraction (SR-PXD) and calorimetric methods. The measured reversible hydrogen storage capacity for the alloys AZ91 and Mg-10 wt.% Gd are 4.2 and 5.8 wt.%, respectively. For the Mg-10 wt.% Gd alloy, the hydrogenated product was also successfully used as starting reactant for the synthesis of $Mg(NH_2)_2$ and as MgH_2 substitute in the Reactive Hydride Composite (RHC) $2LiBH_4 + MgH_2$. The results of this work demonstrate the concrete possibility to use Mg alloy wastes for hydrogen storage purposes.

1. Introduction

Magnesium based alloys find applications in the construction of several products used in our daily life (e.g. automotive application and machinery components). With the advent of light weight/low fuel consumption cars, the overall market for magnesium alloys is destined to grow increasingly. During the manufacture, part of the material is lost as a production waste (e.g. defective parts and shavings). The recycling of the magnesium based wastes is an important issue to be addressed in order to exploit these materials more efficiently. While the industry today effectively recycles the clean process scrap in a closed loop, the challenge is to find a solution to close the loop for the lower grade scrap such as dross, shavings and chips [1]. An interesting possibility is to employ such a waste for producing materials for hydrogen storage. In particular magnesium hydride has the highest energy density of most reversible hydrides applicable for hydrogen storage (9 MJ kg^{-1} Mg) [2]. This material combines a high hydrogen storage capacity of 7.7 wt% with good reversibility [3–11] .

The production costs of materials for hydrogen storage are one of the major barriers to be overcome in order to consider these materials suitable for a large scale application. The utilization of

* Corresponding author.
E-mail addresses: claudio.pistidda@hzg.de, claudio.pistidda@gmail.com (C. Pistidda).

http://dx.doi.org/10.1016/j.jpowsour.2014.07.129
0378-7753/

hydrogen storage systems obtained by recycling of waste magnesium alloys will significantly contribute to the cost reduction of this class of materials. In this work, industrial magnesium based wastes of AZ91 alloy (90 wt.% Mg; 8.71 wt.% Al; 0.66 wt.% Zn; 0.22 wt.% Mn; 0.043 wt.% Si; 0.001 wt.% Fe; 0.002 wt.% Cu and 0.001wt.% Ni) and Mg-10 wt.% Gd alloy (90 wt.% Mg; 10 wt.% Gd) in shaving form were used for the production of hydrogen storage materials. Firstly, the hydrogen sorptive properties of the alloys will be investigated. Secondly, the hydrogenated alloys will be used as starting reactant for the synthesis of further hydrogen storage materials.

Alkali and alkaline earth metal amides, although known since the 19^{h} century and extensively studied for industrials application, only recently have been subject to intensive studies as hydrogen storage systems [12,13]. Magnesium amide, $Mg(NH_2)_2$, and lithium amide, $LiNH_2$, are of currently the most studied amides for hydrogen storage purposes [14–22].

In this work we present results on the synthesis of magnesium amide via reactive ball milling starting from the hydrogenated Mg-10 wt.% Gd alloy and gaseous NH_3.

One of the major issues connected with the storage of hydrogen in metal hydrides and complex metal hydrides is their high thermodynamic stability.

In 1967 Reilly et al. discovered the possibility to change the reaction enthalpy of composites containing hydrides, by mixing them with additives, which react reversibly with the hydride during desorption to form a stable compound. They showed that, at the expense of hydrogen capacity, the reaction enthalpy of a $3MgH_2+MgCu_2$ composite is lowered if compared to pure MgH_2 [23]. Recently, this approach of Reilly et al. has been modified by Chen et al. [14] and later Vajo et al. [24] and Barkhordarian et al. [25], by using hydride mixtures which are also called Reactive Hydride Composites (RHC). This concept offers the advantage to maintain the high gravimetric storage capacity of the single hydrides. Very interesting examples for such hydride mixtures are $2LiBH_4 + MgH_2$ [24–32], and $2NaBH_4 + MgH_2$ [25,33–44]. The mixture $Ca(BH_4)_2 + MgH_2$ [45–48] was also considered as an RHC system, however, it was recently reported that $Ca(BH_4)_2$ and MgH_2 decompose independently from each other. In this work the possibility to substitute MgH_2 with the hydrogenated Mg-10 wt.% Gd alloy in the Reactive Hydride Composite (RHC) $2LiBH_4 + MgH_2$ will be investigated. The material morphology, material composition and sorption behavior of the as received and synthesized materials were investigated by means of scanning electron microscopy coupled with energy dispersive X-ray spectroscopy (SEM-EDS), volumetric measurements, differential thermal analysis (DTA), and *in situ* – *ex situ* XRD techniques.

2. Experimental

Waste AZ91 alloy and Mg-10 wt.% Gd alloy were obtained from the in-house workshop at the Helmholtz-Zentrum Geesthacht in shape of shavings. Before starting this work, the material was stored in air for several months. The alloys were charged into a hardened steel vial and milled for a total time of 1 h in a Spex 8000 ball mill, with a ball to powder ratio of 1:1, using steel spheres with a diameter of 5 mm and weight of 0.4 g. The use of such a ball to powder ratio and balls was chosen to avoid phenomena of cold welding during milling [49]. The milling process was stopped every five minutes and the finest fraction of material was separated with a micro-mesh sieve (mesh size = 125 μm). The portion of material which could not pass trough the sieve was additionally milled for further 5 min in a reiterative process. The milling was performed in a dedicated glove box under a continuously purified argon atmosphere. Based on the van't Hoff equation the equilibrium hydrogen pressure of MgH_2 was calculated to be of 19.49 bar at 400 °C (assuming an enthalpy of formation ΔH_F equal to −74.4 kJ mol^{-1} [50], and entropy of formation ΔS_F of −135 J mol^{-1} K^{-1} [50] for the range of temperatures between 314 and 576 °C). Consequently, in order to achieve a fast hydrogenation kinetic the sieved material was hydrogenated by heat treatment at 400 °C and 50 bar of hydrogen pressure. The material was kept at 400 °C for 5 h and then it was cooled down to room temperature always under a hydrogen pressure of 50 bar. After hydrogenation, the material was milled for additional 5 min as described above.

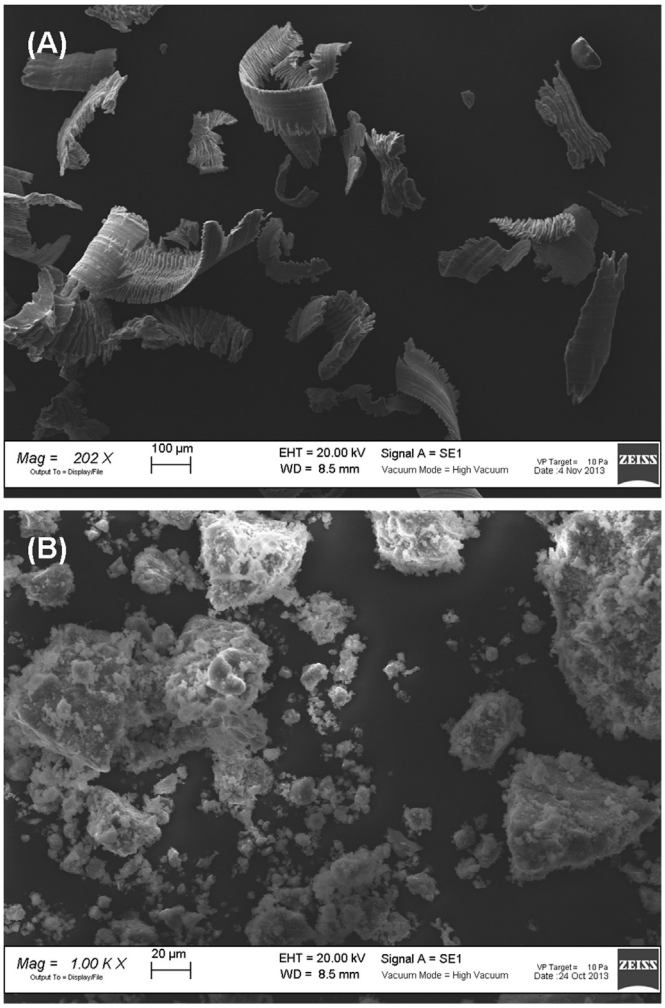

Fig. 1. SEM analysis of the AZ91 alloy as received (A) and after the milling-hydrogenation process (B).

This milling-hydrogenation process was repeated two more times before the material was further characterized.

The reactive ball milling was performed under 7 bar of gaseous NH_3, using a high pressure milling vial from Evico Magnetics and a Fritsch Planetary Mono Mill PULVERISETTE 6. Milling vial and milling tools were made of hardened steel. Half a gram of hydrogenated Mg-10 wt.% Gd alloy was charged in the high pressure milling vial and milled under 7 bar of gaseous NH_3 for 20 h at 300 rpm with a ball to powder ratio of 10:1.

Ex situ powder X-ray diffraction analyses (PXD) were carried out with a Siemens D5000 X-ray diffractometer, using Cu Kα radiation ($\lambda = 1.54056$ Å). The powder was spread onto a silicon single crystal and sealed in the glove box with an airtight hood transparent to the X-rays. *In situ* Synchrotron Radiation Powder X-ray diffraction (SR-PXD) measurements were performed at the MAX II Synchrotron storage ring, at beamline I711 at MAX IV laboratory, Lund, Sweden,

and at the High Resolution Powder Diffraction (HRPD) beamline, PETRA III, Deutsches Elektronen Synchrotron (DESY) Hamburg, Germany. The selected wavelengths were 1.097 and 0.207 Å, respectively. A special sample holder designed for *in situ* monitoring of solid/gas reactions was utilized [26,51–53]. At the HRPD beamline (PETRA III), diffraction patterns were collected on a CsI bonded amorphous Silicon detector, XRD1621 from Perkin Elmer. Sample to Detector Distance (SDD) was calibrated with a LaB_6 standard from NIST. All the raw SR diffraction data were evaluated and converted to 2D powder patterns by the use of FIT2D program [54]. Thermodynamic investigations were performed by differential thermal analysis (DTA, NetzschSTA409). The differential thermal analysis measurements were carried out at the constant argon flow of 50 $ml_n\ min^{-1}$ and with a heating rate of 5 °C min^{-1} in open Al_2O_3 crucibles. Volumetric measurements were performed using a Sievert's type apparatus (Hera, Quebec, Canada). The hydrogen desorption measurements were performed at a hydrogen pressure of 1 bar, heating the material from RT up to 400 °C (heating rate of 3 °C min^{-1}) and then keeping it at 400 °C. The hydrogenation measurements were carried out at a hydrogen pressure of 50 bar, heating the material from 90 °C (Fig. 7) and RT (Fig. 2) up to 400 °C (heating rate of 3 °C min^{-1}) and then keeping it at 400 °C. The morphology and local composition of the material were characterized by scanning electron microscopy (SEM), using an EvoMA10 microscope (Zeiss, Germany) equipped with a LaB_6 filament. To avoid oxidation during the material handling, a special sample holder was used. The sample was loaded into the sample holder in a glove box and afterwards a vacuum was created inside the holder to transport the sample to the SEM.

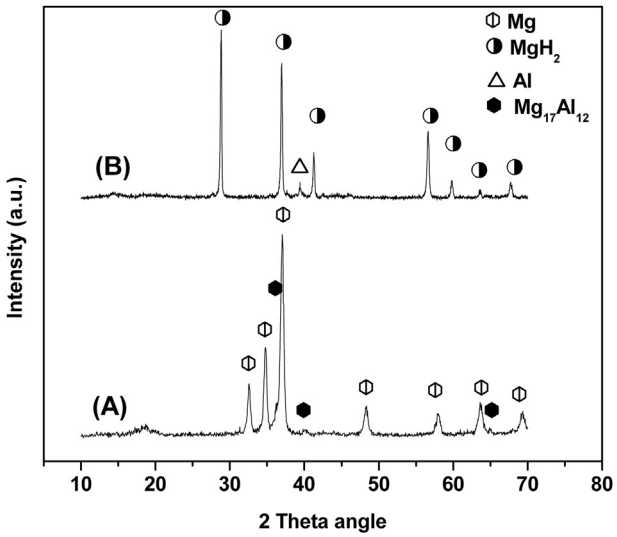

Fig. 3. XRD patterns of the AZ91 alloy as received (A) and after full hydrogenation at 400 °C and 50 bar of hydrogen (λ = 1.54056 Å) (B).

3. Results

The SEM characterization of the AZ91 alloy as received from the workshop and after complete milling-hydrogenation process is reported in Fig. 1, picture A and B respectively. The as received

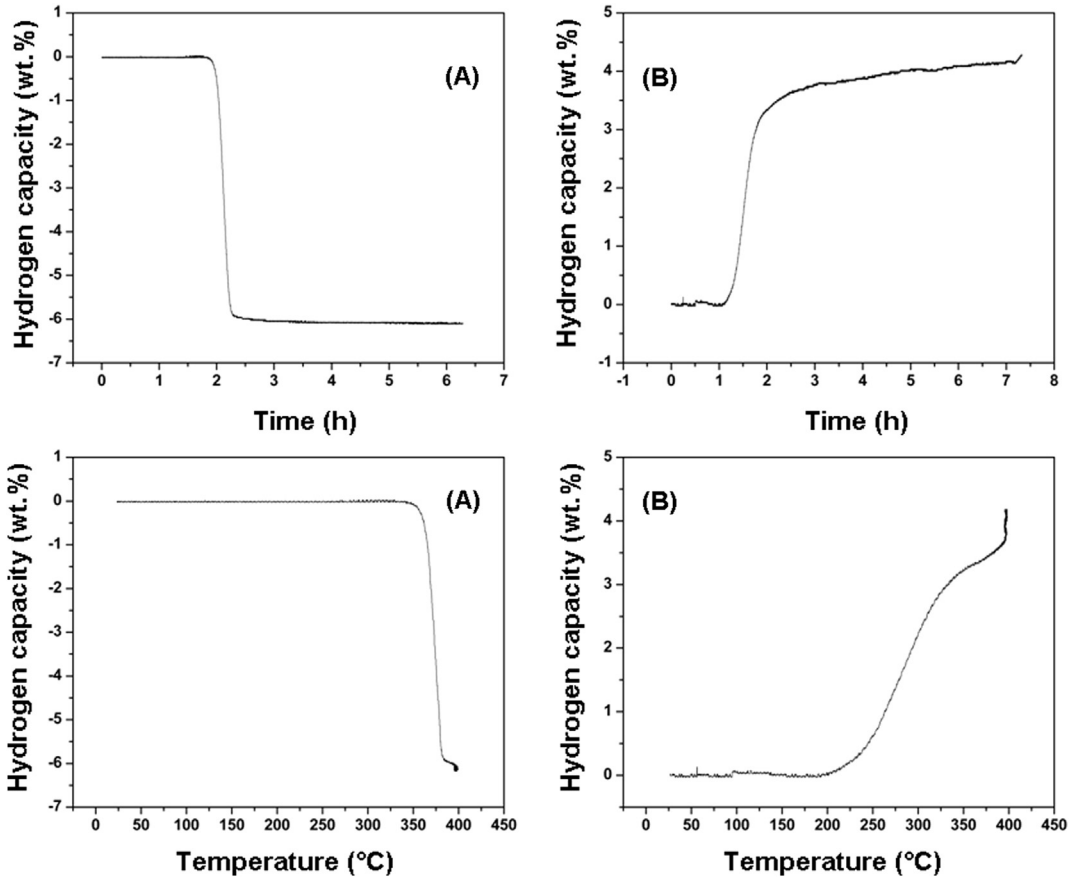

Fig. 2. Hydrogen desorption kinetics of the milled-hydrogenated AZ91 alloy (A). The sample was heated under 1 bar hydrogen pressure from RT to 400 °C (heating rate of 3 °C min^{-1}). Hydrogen absorption kinetic of the desorbed AZ91 alloy (B). The sample was heated under 50 bar hydrogen pressure from RT to 400 °C (heating rate of 3 °C min^{-1}).

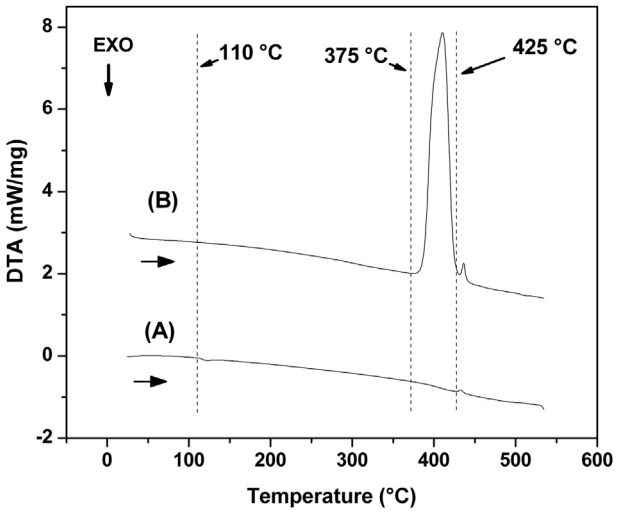

Fig. 4. DTA traces for the AZ91 alloy as received (A) and after the milling-hydrogenation process (B), measured under an argon flow of 50 mL min^{-1} from RT to 550 °C (5 °C min^{-1} heating).

material consists of alloy shavings of several hundreds of micrometers of dimension. After the milling-hydrogenation process, the morphology of the material drastically changes. The hydrogenated material appears powdery and the dimension of the particles is between 5 μm to roughly 100 μm.

The hydrogen sorption properties of the AZ91 alloy were investigated by means of volumetric technique. Fig. 2(A) shows the desorption kinetics of the hydrogenated AZ91 alloy. The material appears to be stable up to 350 °C were the material starts to release hydrogen. The hydrogen desorption reaction takes place in a single step and it is complete in only a few minutes. The final amount of hydrogen released is equal to 6.25 wt.%. The re-hydrogenation of the desorbed material is shown in Fig. 2(B). The material starts to absorb hydrogen at roughly 200 °C. The absorption reaction continues during the remaining heating period and the following hours of isothermal treatment at 400 °C, reaching the final amount of stored hydrogen equal only to 4.2 wt.%.

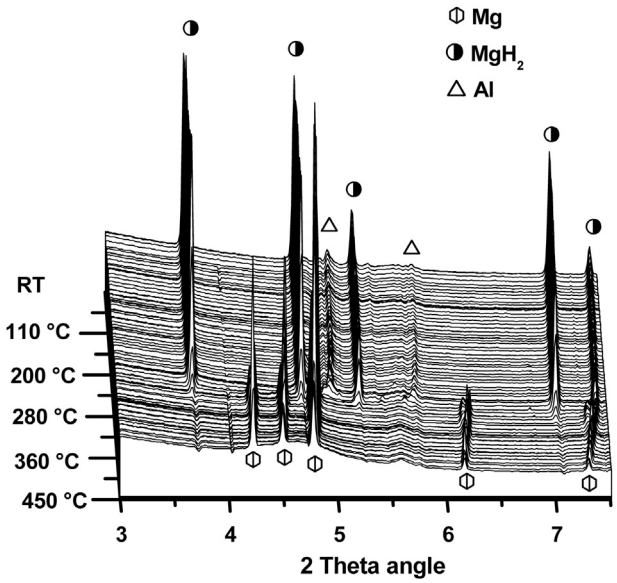

Fig. 5. Series of SR-PXD patterns of the milled-hydrogenated AZ91 magnesium alloy. The sample was heated under 1 bar hydrogen pressure from RT to 450 °C (heating rate of 3 °C min^{-1}; $\lambda = 0.207$ Å).

The AZ91 alloy as received and after hydrogenation at 400 °C and 50 bar of hydrogen was also characterized by XRD technique (Fig. 3). In the diffraction pattern of the as received alloy the peaks of Mg and $Mg_{17}Al_{12}$ are visible. No traces of MgO and of the other alloying elements or derivate of the alloying elements are observed. The diffraction pattern of the hydrogenated alloy shows the presence of beta-MgH_2 and Al. Hence, the conversion of the starting Mg and Mg contained in the $Mg_{17}Al_{12}$ alloy into beta-MgH_2 is complete.

In order to gain insight into the hydrogen desorption properties of the AZ91 alloy, the as received AZ91 alloy as well as after the milling-hydrogenation process were characterized by DTA technique (Fig. 4, respectively trace A and B). The measurements were performed heating the samples from room temperature up to 550 °C. In trace A, upon heating two small signals, one exothermic with onset temperature at 110 °C and one endothermic at 425 °C, are detectable. These signals can be attributed to the reaction of the water physisorbed on the surface of the material with the material and to the melting of a small portion of the alloy, respectively. Trace B shows upon heating a major endothermic signal with onset temperature at 375 °C, followed by a second small endothermic signal which, as for the as received alloy, has onset temperature at 425 °C. The cooling portions of both the traces are omitted because they did not show relevant events.

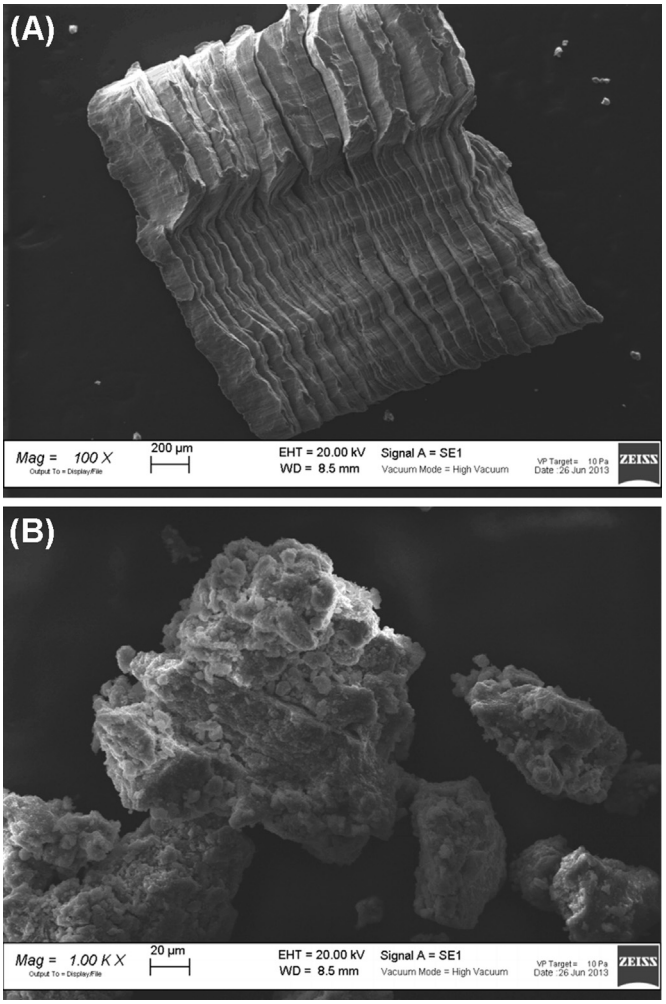

Fig. 6. SEM analysis of the Mg-10 wt.% Gd alloy as received (A) and after the milling-hydrogenation process (B).

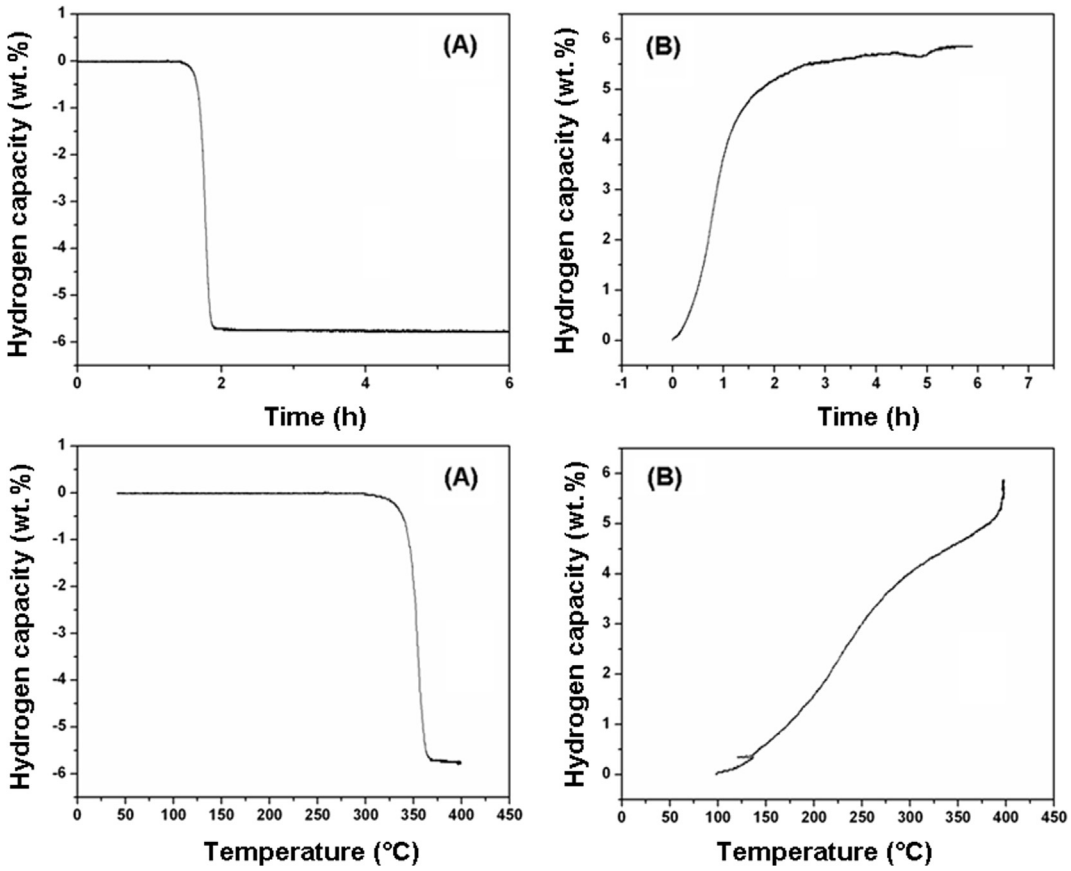

Fig. 7. Hydrogen desorption kinetics of the milled-hydrogenated Mg-10 wt.% Gd alloy (A). The sample was heated under 1 bar hydrogen pressure from RT to 400 °C (heating rate of 3 °C min^{-1}). Hydrogen absorption kinetic of the desorbed Mg-10 wt.% Gd alloy (B). The sample was heated under 50 bar hydrogen pressure from 90 to 400 °C (heating rate of 3 °C min^{-1}).

Fig. 5 shows the *in situ* SR-PXD characterization of the hydrogen desorption process of the hydrogenated AZ91 alloy. The measurement was carried out at the hydrogen pressure of 1 bar, heating the material from room temperature up to 450 °C. As previously seen in the diffraction pattern B of Fig. 3, the visible diffracted peaks can be attributed to the presence of magnesium hydride and a small amount of Al. Due to thermal expansion of the unit cells, all the corresponding peaks shift toward lower 2 Theta angle upon heating. The intensity of the peaks of MgH_2 starts to decrease at about 370 °C. Simultaneously with the MgH_2 disappearance and consequent formation of free Mg, the main visible peaks of Al also disappear. The decomposition of beta-MgH_2 is complete at 390 °C.

Fig. 6 shows the SEM characterization of the Mg-10 wt.% Gd alloy as received and after the milling–hydrogenation process, picture A and B respectively. The as received material consists of alloy shavings of several millimeters of dimension. As a consequence of the milling–hydrogenation process, the morphology of the material significantly changes. The hydrogenated material appears powdery and the average dimension of the particles is around 100 μm.

Fig. 7(A) shows the desorption kinetics of the hydrogenated Mg-10 wt.% Gd alloy. The material appears to be stable up to 310 °C: at this temperature the material starts to release hydrogen. The hydrogen desorption reaction takes place in a single step and it is complete at roughly 370 °C. The final amount of hydrogen released is equal to 5.8 wt.%. As for the AZ91 alloy, an attempt to re-hydrogenate the desorbed material was made (Fig. 2(B)). Surprisingly, the material starts to absorb hydrogen, although in moderate amount, already at 90 °C. The absorption reaction continues during the heating period and the following 5 h of isothermal treatment at 400 °C, reaching the final amount of stored hydrogen equal to 5.8 wt.%.

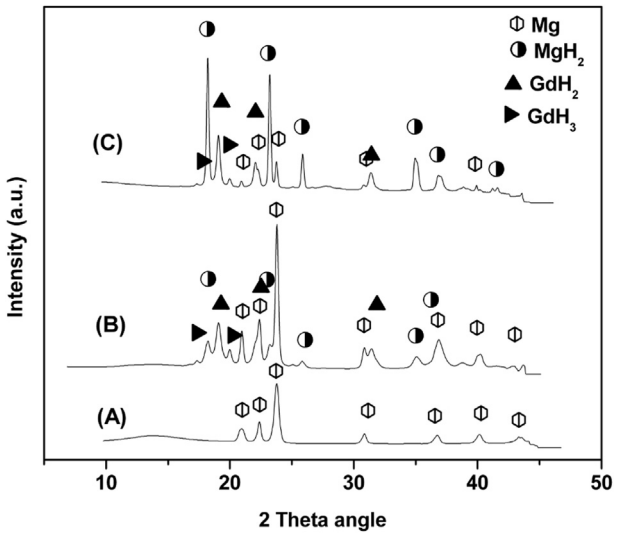

Fig. 8. XRD patterns of the Mg-10 wt.% Gd alloy as received (A), after partial hydrogenation at 150 °C and 50 bar of hydrogen, and after full hydrogenation at 400 °C and 50 bar of hydrogen (C); $\lambda = 0.939$ Å.

In order to understand the reason behind the hydrogenation of Mg-10 wt.% Gd alloy at the low temperature, XRD characterization was carried out (Fig. 8). The diffraction patterns of the material as received, heated up to 150 °C (heating rate of 3 °C min^{-1}) at 50 bar of hydrogen pressure, and fully hydrogenated at 400 °C and 50 bar of hydrogen pressure are displayed in Fig. 8(A) and (B), respectively. In the diffraction pattern A only the Bragg reflections of magnesium are visible. The pattern acquired for the material heated up to 150 °C under 50 bar of hydrogen pressure shows the presence of beta-MgH_2, GdH_2 and GdH_3 plus un-reacted Mg. The formation of these hydride phases clearly justifies the hydrogen absorption at low temperature, observed for the volumetric analysis presented in Fig. 7. Finally, the diffraction pattern of the fully hydrogenated material shows almost complete conversion of the starting Mg (still visible) into beta-MgH_2, plus the reflections of GdH_2 and GdH_3.

The hydrogen desorption reaction of the hydrogenated Mg-10 wt.% Gd alloy was studied also by DTA technique. Fig. 9 shows the DTA traces of the as received alloy (trace A) and of the hydrogenated material (trace B). The measurements were performed heating the sample from room temperature up to 650 °C. The trace of the as received alloy shows a single endothermic signal with onset at 600 °C. This signal can be attributed to the melting of a portion of the sample, as it is deducible from the binary Mg-Gd phase diagram [55]. The DTA trace of the hydrogenated material shows the first endothermic signal with onset at 375 °C, followed by the endothermic signal of the partial melting of the alloy at 600 °C. The signal at 375 °C is related to the hydrogen release from the material; however, it is interesting to notice that in this case the reaction onset is at a temperature which is roughly 65 °C higher than that observed in the volumetric analysis of Fig. 7(A) (310 °C). In fact, being the volumetric analysis performed under hydrogen back pressure, we expected the onset temperature of the volumetric analysis to be shifted to a temperature higher than that observed in the DTA measurement.

Fig. 10 shows the *in situ* SR-PXD analysis of the hydrogen desorption process of the hydrogenated Mg-10 wt.% Gd alloy. The measurement was performed at the hydrogen pressure of 1 bar, heating up the material from room temperature up to 400 °C and then keeping it under isothermal conditions for several minutes. As observed in Fig. 8 pattern C, the starting material consist of a mixture of beta-MgH_2, GdH_2, GdH_3 plus a small amount of un-

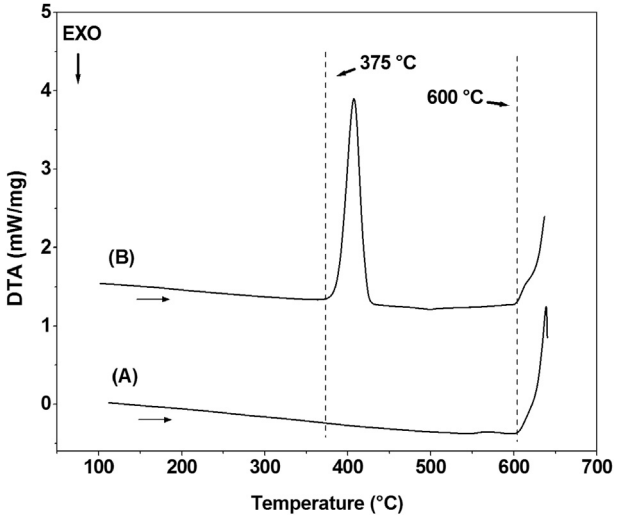

Fig. 9. DTA traces of the Mg-10 wt.% Gd alloy as received (A) and after the milling-hydrogenation process (B), measured under an argon flow of 50 mL min^{-1} from RT to 650 °C (5 °C min^{-1} heating rate).

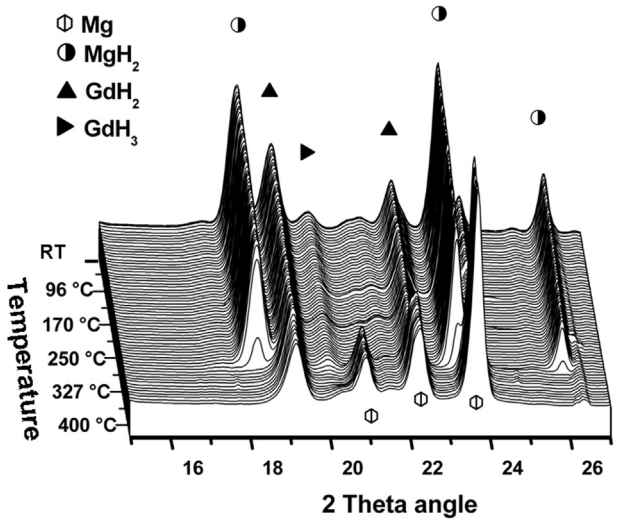

Fig. 10. Series of SR-PXD patterns of the milled- hydrogenated Mg-10 wt.% Gd alloy. The sample was heated under 1 bar hydrogen pressure from RT to 400 °C (heating rate of 3 °C min^{-1}; λ = 1.097 Å).

reacted Mg. Upon heating, a continuous shift of all the peaks towards lower 2 Theta angle is visible due to expansion of the unit cells. The phases appear to be stable up to 315 °C after which the intensity of beta-MgH_2 and GdH_3 reflections start to decrease, and they completely disappear at around 350 °C. Simultaneously with the MgH_2 disappearance, the reflections of Mg rise. Although it is not clearly visible, it is possible to assume that GdH_3 partially desorbs hydrogen to form GdH_2, which appears stable during the heating and subsequent isothermal period at 400 °C.

Under the conditions applied in this study the alloy AZ91 shows higher first hydrogen desorption capacity with respect to the alloy Mg-10 wt.% Gd, but during the re-hydrogenation process, the hydrogen capacity is considerably reduced, whereas in the case of Mg-10 wt.% Gd alloy, the full amount of hydrogen could be restored. For this reason the hydrogenated alloy Mg-10 wt.% Gd was chosen as starting reactant for the synthesis of further hydrogen storage systems.

Magnesium amide $Mg(NH_2)_2$ has recently been studied as hydrogen storage material alone and in combination with other hydrides [56–58]. In the following, an attempt of synthesizing magnesium amide starting from hydrogenated Mg-10 wt.% Gd alloy via reactive ball milling in gaseous NH_3 is reported, described by the equation below:

$$MgH_2 + 2NH_3 \rightarrow Mg(NH_2)_2 + 2H_2. \quad (1)$$

The black color of the starting material changes during milling, since, the milling product appears bright gray and the material volume largely increased.

The decomposition process of the ball milled material was investigated via DTA technique. In Fig. 11, the DTA traces of the ammoniated Mg-10 wt.% Gd alloy (trace A) and of pure gadolinium hydride (GdH_2), milled in ammonia atmosphere with the same parameters as used for the hydrogenated Mg-10 wt.% Gd alloy (trace B), are presented. The measurements were performed heating the samples from RT up to 490 °C and then cooling them down to RT again. Trace A shows three main signals occurring during the heating process: one exothermic with onset at 275 °C and two endothermic with onsets at 328 and 459 °C. The cooling part of trace A does not show significant events. In trace B no signals are visible, neither upon heating nor during cooling.

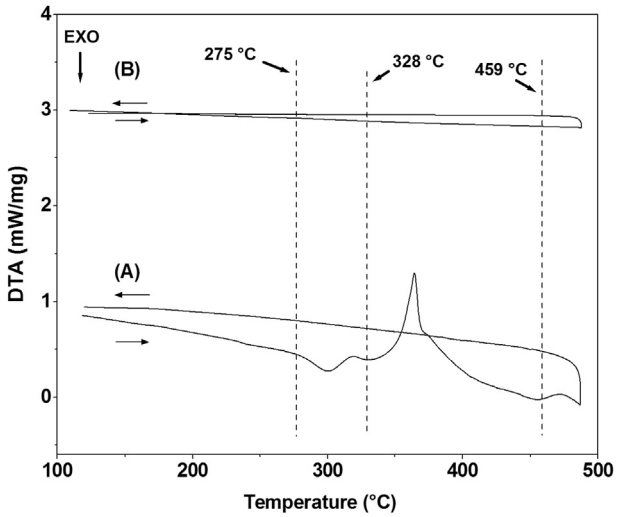

Fig. 11. DTA traces of the ammoniated hydrogenated Mg-10 wt.% Gd alloy (A) and of pure gadolinium hydride (GdH_2) milled in ammonia atmosphere (B), measured under an argon flow of 50 mL min^{-1} from RT to 490 °C and back to RT (5 °C min^{-1} heating-cooling rate).

To understand the nature of the signal observed in Fig. 11, XRD characterization of ammoniated Mg-10 wt.% Gd alloy was carried out (Fig. 12). In the diffraction pattern of ammoniated Mg-10 wt.% Gd (A), only the weak diffraction peaks of GdN are visible. A portion of the ammoniated material was heated up to 310 °C under argon atmosphere. In the DTA (trace A of Fig. 11), these conditions correspond to the end of the exothermic signal observed upon heating. The diffraction analysis of this material (pattern B) shows the clear presence of $Mg(NH_2)_2$. The diffraction pattern of the material after complete desorption at 450 °C at 1 bar of hydrogen pressure (pattern C) shows only the presence of Mg_3N_2. In pattern B and C, the diffraction peaks of GdN are not visible anymore because of the overlap with the peaks of the predominant $Mg(NH_2)_2$ and Mg_3N_2.

In order to investigate the possibility of replacing the high purity beta-MgH_2 with hydrogenated Mg-10 wt%Gd waste alloy in the RHC systems, the mixture $2LiBH_4+MgH_2$ was chosen. The mixture was prepared by ball milling two mol of $LiBH_4$ together with a mol of the hydrogenation Mg-10 wt.% Gd and 2.5 mol% of $TiCl_3$ for five hours in a Spex 8000 ball mill, with a ball to powder ratio of 10:1. The addition of $TiCl_3$ to $2LiBH_4+MgH_2$ was reported to be beneficial for the hydrogen sorption properties of this system [59]. The first hydrogen desorption and the first hydrogen absorption of the obtained $LiBH_4$-hydridized Mg-10 wt.% Gd mixture is shown in Fig. 13. The desorption measurement was performed heating up the material from room temperature up to 400 °C with a heating rate of 3 °C min^{-1} and then keeping the material under isothermal conditions at 400 °C for several hours. The measurement was carried out at a hydrogen pressure of 3 bar. The desorption process starts during the heating period at about 300 °C and continues during the isothermal period at 400 °C, releasing in a first step an amount of hydrogen equal to roughly 2.5 wt.% and in the second step an additional 5 wt.%. After desorption, the material underwent a re-hydrogenation process at the constant temperature of 350 °C and 50 bar of hydrogen pressure. The absorption reaction took place in a single step charging within seven hours an amount of hydrogen equal to that released in the previous desorption (i.e. 7.5 wt.%). Hence, the system is fully reversible.

The XRD characterization of the $LiBH_4$-hydridized Mg-10 wt.% Gd mixture upon cycling is shown in Fig. 14. In the diffraction pattern of the as milled material (pattern A) the reflections of the orthorhombic $LiBH_4$, beta-MgH_2, GdH_2 and LiCl are visible. The LiCl phase is formed by reaction of the $TiCl_3$ with the $LiBH_4$. The hydrogen desorption of the as milled material at 3 bar of hydrogen pressure and at a temperature of 400 °C lead to the formation of MgB_2, Mg and LiH, GdH_2 and LiCl appear to be stable (pattern B). The pattern of the material after the re-hydrogenation process at 350 °C and 50 bar of hydrogen pressure (pattern C) shows the presence of the orthorhombic $LiBH_4$, beta-MgH_2, beside the reflections of GdH_2 and LiCl. The diffracted intensity of this last pattern was multiplied by a factor of 0.5. The re-hydrogenated material appears highly heterogeneous, since, the portion of the sample rich in $LiBH_4$ appears glassy and made of big particles, whereas the portion of sample rich in MgH_2 is powdery.

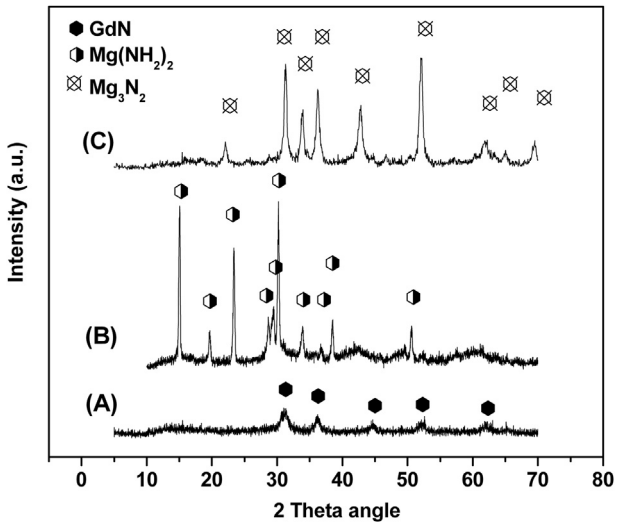

Fig. 12. XRD patterns of the ammoniated hydrogenated Mg-10 wt.% Gd alloy (A), ammoniated hydrogenated Mg-10 wt.% Gd alloy after heating up to 310 °C under argon atmosphere (B) and ammoniated hydrogenated Mg-10 wt.% Gd alloy after complete desorption at 450 °C at 1 bar of hydrogen pressure (λ = 1.54056 Å).

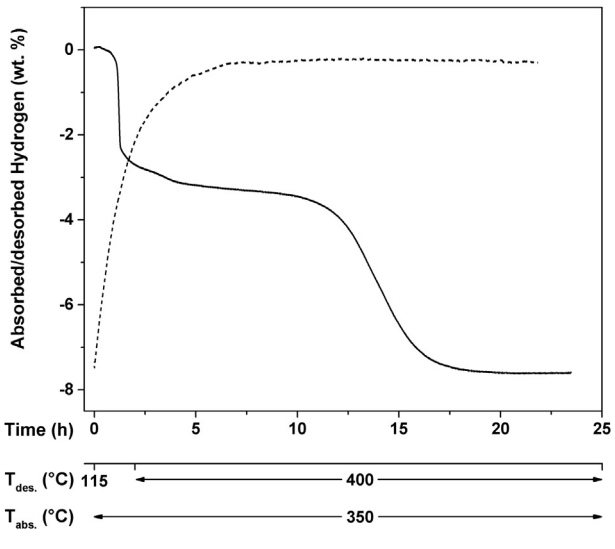

Fig. 13. Hydrogen desorption kinetic of the as milled $LiBH_4$-hydrogenatedMg-10 wt.% Gd mixture. The sample was heated under 3 bar hydrogen pressure from RT to 400 °C (heating rate of 3 °C min^{-1}). Hydrogen absorption kinetic of the desorbed $LiBH_4$-hydrogenated Mg-10 wt.% Gd mixture. The sample was kept for several hours under 50 bar of hydrogen pressure at 350 °C.

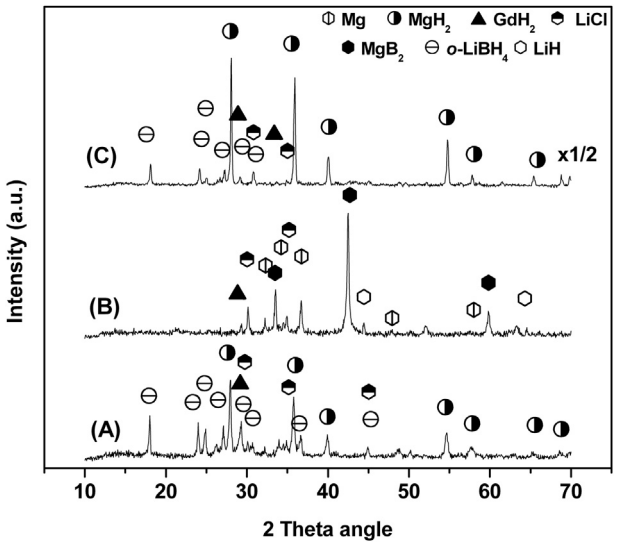

Fig. 14. XRD patterns of the as milled $LiBH_4$-hydrogenated Mg-10 wt.% Gd mixture (A), $LiBH_4$-hydrogenated Mg-10 wt.% Gd mixture after hydrogen desorption at 400 °C and 3 bar of H_2 pressure (B) and $LiBH_4$-hydrogenated Mg-10 wt.% Gd mixture after re-hydrogenated at 350 °C and 50 bar of H_2 pressure ($\lambda = 1.54056$ Å).

4. Discussion

The results presented above demonstrate that the use of magnesium industrial wastes for hydrogen storage purposes is possible and easily achievable.

As discussed in the experimental section, a preliminary ball milling-separation-hydrogenation process was carried out. This first step in the material preparation was employed in order to obtain a fine and reactive alloy powder. In fact, before starting this work, the materials (the shavings of the alloys AZ91 and Mg-10 wt.% Gd) were stored in air and, as previously reported in several publications concerning Mg and Mg alloys, it is likely that an insulating layer of few nano-meters of magnesium oxide/magnesium hydroxide was present at the topmost part of the material surface [60–70]. In addition, it is well known from the literature that in the early instants of the hydrogenation of the magnesium fraction of the alloys, the hydrogenation process is limited by the hydrogen dissociation on the magnesium surface [6]. Therefore, the employment of the ball milling technique, to reduce the particle size of the alloys and to break the passivating oxide/hydroxide layer, greatly improved the kinetics and completeness of hydrogenation.

The theoretical hydrogen storage capacities of the AZ91 and Mg-10 wt.% Gd alloys (6.9 and 7.1 wt.%, respectively) were calculated based on their nominal chemical composition. Magnesium alloy names are often given by two letters followed by two numbers. Letters stand for the alloying elements (A = aluminium, Z = zinc, M = manganese, S = silicon). Numbers indicate respective nominal compositions of main alloying elements. The acronym AZ91, for example, denotes an magnesium alloy with roughly 9 wt.% aluminium and 1 wt.% zinc. In fact, the exact composition of the alloy AZ91 is 90 wt.% Mg; 8.71 wt.% Al; 0.66 wt.% Zn; 0.22 wt.% Mn; 0.043 wt.% Si; 0.001 wt.% Fe; 0.002 wt.% Cu and 0.001wt.% Ni, whereas the Mg-10 wt.% Gd alloy consists of 90 wt.% Mg and 10 wt.% Gd. For the AZ91 alloy we considered the hydrogen capacity to depend only on the formation of beta-MgH_2, and for the Mg-10wt.% Gd alloy on the formation of beta-MgH_2 and GdH_3. Although these are the nominal compositions, the real compositions of the as received waste material might differ slightly due to burn off phenomena during melting and material reaction with the reactor walls upon alloy synthesis and casting. This would partially explain the reason for not achieving the expected gravimetric hydrogen capacity, in particular in the case of the alloy AZ91 (Fig. 2). In fact, for this alloy the XRD pattern of the hydrogenated material shows a full conversion of all the Mg present in the alloy into beta-MgH_2 (Figs. 3 and 5), whereas in the case of the Mg-10 wt.% Gd alloy, the unachieved storage capacity (Fig. 7) is mostly due to incomplete conversion of the starting Mg into beta-MgH_2 (Figs. 8 and 10). This effect was already described in literature for the hydrogenation of pure Mg: if the Mg particles are relatively large, the growing MgH_2 layer on the surface of these particles acts as diffusion barrier for the hydrogen hindering the absorption process [10].

Despite the differences of composition between the two alloys, the desorption kinetics are similar. In fact, in both cases the hydrogen desorption takes place in a single step and it is complete in a time period of approximately five minutes.

The earlier beginning of the desorption reaction in the case of the hydrogenated AZ91 alloy compared to the hydrogenated Mg-10 wt.% Gd alloy (~50 °C) can be explained by the presence of Al. In fact, compared to pure magnesium the plateau pressure of Mg–Al alloys are generally higher, therefore, the presence of Al in the AZ91 alloy might facilitate the MgH_2 decomposition reaction [71].

After dehydrogenation, the following hydrogenation of the AZ91 alloy shows a significant reduction of the achieved hydrogen capacity (−33% of the capacity measured during desorption).

Beside a possible massive growth of the alloy particles and crystallites, the presence of $Mg_{17}Al_{12}$ in equilibrium with Mg in the alloy AZ91 can partially justify the reduction of hydrogen storage capacity. The hydrogenation reaction of the alloy $Mg_{17}Al_{12}$ is described by the two simplified following equations [72–75]:

$$Mg_{17}Al_{12} + 9H_2 \leftrightarrow 9MgH_2 + 4Mg_2Al_3 \quad (2)$$

$$4Mg_2Al_3 + 8H_2 \leftrightarrow 8MgH_2 + 12Al \quad (3)$$

The enthalpies of reaction for the two hydrogenation steps are -72 ± 2 kJ mol^{-1} H_2 and -62 ± 2 kJ mol^{-1} H_2, respectively for step 1 and step 2 [73]. Consequently, considering the final hydrogenation temperature used for the hydrogenation process shown in Fig. 2 (i.e. 400 °C) only the first step of hydrogenation of $Mg_{17}Al_{12}$ is possible.

Although the preliminary hydrogenation of the alloy AZ91 was carried out also at a temperature of 400 °C and 50 bar of hydrogen, its diffraction pattern (Fig. 3(B)) shows a complete conversion of the starting material into MgH_2 and Al. This is due to the fact that after the hydrogenation the complete material was cooled down to room temperature under a constant hydrogen pressure of 50 bar, therefore, the hydrogenation of Mg_2Al_3 (equation (2)) took place at a temperature equal to or lower than 330 °C.

After the first hydrogen desorption, the subsequent hydrogenation of Mg-10 wt.% Gd alloy shows a full reversibility. Interestingly, the desorbed Mg-10 wt.% Gd alloy starts to absorb hydrogen already at 90 °C under a hydrogen pressure of 50 bar and reaches a capacity of stored hydrogen equal to 0.6 wt.% already at 150 °C. The desorbed AZ91 under the same hydrogen pressure conditions starts to absorb hydrogen at roughly 200 °C. Assuming that all Gd present in the desorbed state of the hydrogenated Mg-10 wt.% Gd alloy is confined to GdH_2, the absorption of hydrogen at low temperature might be explained by a possible catalytic effect of GdH_2 in facilitating the dissociation of H_2 and the diffusion of the H atoms. This would also justify the complete reversibility of the hydrogenation process of the Mg-10 wt.% Gd alloy. A similar behavior was observed by Couillaud et al. [76] during the investigation of the

hydrogen sorption properties of the alloy $Gd_{13}Ni_9Mg_{78}$. In addition, also other hydrides of rare earth elements ("REEs") were found to play an important role in improving the sorption properties of Mg-based systems (e.g. YH_3) [77–79].

As explained in the experimental section, due to the possibility to be fully re-hydrogenated, the Mg-10 wt.% Gd alloy in the hydrogenated state was chosen as starting reactant for the synthesis of further hydrogen storage systems.

The ball milling technique in NH_3 atmosphere is considered as an effective method for the synthesis of metal amides [80]. Compared to the heating in NH_3 atmosphere, the milling process leads to an acceleration of the reaction between metal hydrides and gaseous NH_3 [80,81]. This is clearly due to the continuous opening of fresh and reactive surfaces between metal hydrides and NH_3 [49]. The milling of the hydrogenated Mg-10 wt.% Gd alloy in ammonia atmosphere clearly lead to the formation of GdN and nano-structured $Mg(NH_2)_2$ (Fig. 12 pattern A). In fact, the diffraction pattern of the material heated up to 310 °C (Fig. 12 pattern B) shows the formation of crystalline $Mg(NH_2)_2$, identifying the endothermic peak with the onset temperature of 275 °C in the corresponding DTA trace (Fig. 11 pattern A) to be the crystallization of $Mg(NH_2)_2$. Further heating to 450 °C leads to the decomposition of $Mg(NH_2)_2$ forming Mg_3N_2 (Fig. 12 pattern C). The absence of any beta-MgH_2 reflection in the ammoniated material (Fig. 12) is a clear indication of the complete conversion of the starting Mg containing phases of the hydrogenated Mg-10 wt.% Gd alloy into $Mg(NH_2)_2$.

The attempt of substituting pure beta-MgH_2 with hydrogenated Mg-10 wt.% Gd alloy in the system $2LiBH_4+MgH_2$ was successfully carried out. The hydrogen desorption and absorption reactions proceed as reported in literature in two steps and one step, respectively [26]. The first desorption step is associated with the decomposition of MgH_2, whereas the second is related to the desorption of $LiBH_4$. Due to kinetic limitations (nucleation restriction of MgB_2, low mobility of atoms and large diffusion paths), the second release of hydrogen occurs in the isothermal region after an incubation period of several hours. However, upon absorption the formation of $LiBH_4$ and MgH_2 occurs simultaneously. Despite a theoretical hydrogen capacity of roughly 11 wt.% (value calculated based on the hydrogen capacity of only $LiBH_4$ and MgH_2), the measured capacity is 7.5 wt% (Fig. 13). The formation of LiCl at the expenses of $LiBH_4$ and $TiCl_3$ is one of the reasons for not achieving the theoretical hydrogen capacity (Fig. 14). A side reaction between GdH_3 and $LiBH_4$ to form gadolinium borides during milling is possible. In fact, only the Bragg reflections of GdH_2 are well visible in the patterns reported in Fig. 14. The XRD pattern of the material re-hydrogenated shows anomaly small reflections of $LiBH_4$ (pattern C). This is due to the strong heterogeneity of the material after re-hydrogenation which did not allow sampling the material in a representative way. Based on our observations, we can state that the material heterogeneity is a direct consequence of the fact that at the temperature of re-hydrogenation a portion of the sample is in a solid state (i.e. Mg, MgH_2, LiCl, GdH_2) whereas another is in a molten state (i.e. $LiBH_4$). During the re-hydrogenation process, the portion of the material in the molten state tends to separate from the material in a solid state. This separation is normally preserved during cooling.

5. Conclusion

In this work, industrial low grade wastes of magnesium alloys AZ91 and Mg-10 wt.% Gd were successfully used for the production of hydrogen storage materials. Despite being stored for long time in air, the alloys, after a preliminary ball milling-separation/ball milling hydrogenation process, readily takes up hydrogen. At front of a theoretical hydrogen capacity of 6.9 wt.% for the alloy AZ91 and 7.1 for the alloy Mg-10 wt.% Gd, the achieved hydrogen storage capacities were 6.25 and 5.8 wt.%, respectively. Surprisingly, under a hydrogen pressure of 50 bar the Mg-10 wt.% Gd alloy starts to absorb hydrogen already at 90 °C. This phenomenon was attributed to a possible catalytic effect of GdH_2 in facilitating the dissociation of H_2 and the diffusion of the atomic hydrogen. The hydrogenated Mg-10 wt.% Gd alloy was successfully employed as a starting reactant for the synthesis of magnesium amide by ball milling in ammonia atmosphere. A full conversion of the beta-MgH_2 into $Mg(NH_2)_2$ was achieved. In addition, the use of hydrogenated Mg-10 wt.% Gd alloy as MgH_2 substitute in the RHC system $2LiBH_4+MgH_2$ was also tested. Although, due to possible side reaction between the alloy components and $LiBH_4$, the capacity of the obtained system was lower than the expected one, an amount of hydrogen equal to 7.5 wt.% was reversibly stored in the system. The results showed in this work demonstrate that the use of low grade waste magnesium alloys as hydrogen storage material and/or as reactants for the production of further hydrogen storage systems is possible and easily achievable.

Acknowledgments

The work was supported by the Danish National Research Foundation, Center for Materials Crystallography (DNRF93), the Danish Strategic Research Council (the research project HyFillFast), and by the Danish Research Council for Nature and Universe (Danscatt). We are grateful to the Carlsberg Foundation. The access to beamtime at the MAX-II synchrotron, Lund, Sweden in the research laboratory MAX-lab is gratefully acknowledged.

We also acknowledge funding from the European Community's Seventh Framework Programme, The Fuel Cells and Hydrogen Joint Undertaking (FCH JU), project BOR4STORE (303428) and the COST Action MP1103 "Nanostructured materials for solid-state hydrogen storage".

References

[1] H. Westengen, Recycling, in: B.L.M. Horst, E. Friedrich (Eds.), Magnesium Technology, 2006, pp. 633–664.
[2] B. Sakintuna, F. Lamari-Darkrim, M. Hirscher, Int. J. Hydrogen Energy 32 (2007) 1121–1140.
[3] R. Wiswall, Top. Appl. Phys. 29 (1978) 209.
[4] A. Zaluska, L. Zaluski, J.O. Ström-Olsen, J. Alloy. Compd. 288 (1999) 217–225.
[5] S. Deledda, A. Borissova, C. Poinsignon, W.J. Botta, M. Dornheim, T. Klassen, J. Alloy. Compd. 404 (2005) 409–412.
[6] M. Dornheim, S. Doppiu, G. Barkhordarian, U. Bösenberg, T. Klassen, O. Gutfleisch, R. Börmann, Scr. Mater. 56 (2007) 841–846.
[7] O. Friedrichs, T. Klassen, J.C. Sánchez-López, R. Börmann, A. Fernández, Scr. Mater. 54 (2006) 1293–1297.
[8] O. Friedrichs, J.C. Sánchez-López, C. López-Cartes, M. Dornheim, T. Klassen, R. Börmann, A. Fernández, Appl. Surf. Sci. 252 (2006) 2334–2345.
[9] P.A. Huhn, M. Dornheim, T. Klassen, R. Börmann, J. Alloy. Compd. 404 (2005) 499–502.
[10] C.M. Stander, Z. Phys. Chem. 104 (1977) 229–238.
[11] C.M. Stander, J. Inorg. Nucl. Chem. 39 (1977) 221–223.
[12] L.J. Thénard, J.L. Gay-Lussac, Rech. Physicochim. I (1811), 337, 341, 354, 356.
[13] A.W. Titherley, J. Chem. Soc. 65 (1894) 504–522.
[14] P. Chen, Z. Xiong, J. Luo, J. Lin, K.L. Tan, Nature 420 (2002) 302–304.
[15] P. Chen, Z. Xiong, J. Luo, J. Lin, K.L. Tan, J. Phys. Chem. B 107 (2003) 10967–10970.
[16] J. Hu, G. Wu, Y. Liu, Z. Xiong, P. Chen, K. Murata, K. Sakata, G. Wolf, J. Phys. Chem. B 110 (2006) 14688–14692.
[17] H. Leng, T. Ichikawa, H. Fujii, J. Phys. Chem. B 110 (2006) 12964–12968.
[18] H.Y. Leng, T. Ichikawa, S. Hino, N. Hanada, S. Isobe, H. Fujii, J. Phys. Chem. B 108 (2004) 8763–8765.
[19] W. Luo, J. Alloy. Compd. 381 (2004) 284–287.
[20] W. Luo, S. Sickafoose, J. Alloy. Compd. 407 (2006) 274–281.
[21] Y. Nakamori, G. Kitahara, K. Miwa, S. Towata, S. Orimo, Appl. Phys. A 80 (2005) 1–3.
[22] Z. Xiong, G. Wu, J. Hu, P. Chen, Adv. Mater. 16 (2004) 1522–1525.
[23] J.J. Reilly, R.H. Wiswall, Inorg. Chem. 7 (1968) 2254–2256.
[24] J.J. Vajo, F. Mertens, C.C. Ahn, R.C. Bowman, B. Fultz, J. Phys. Chem. B 108 (2004) 13977–13983.

[25] G. Barkhordarian, T. Klassen, M. Dornheim, R. Börmann, J. Alloy. Compd. 440 (2007) L18–L21.
[26] U. Bösenberg, S. Doppiu, L. Mosegaard, G. Barkhordarian, N. Eigen, A. Borgschulte, T.R. Jensen, Y. Cerenius, O. Gutfleisch, T. Klassen, M. Dornheim, R. Börmann, Acta Mater. 55 (2007) 3951–3958.
[27] U. Bösenberg, J.W. Kim, D. Gosslar, N. Eigen, T.R. Jensen, J.M.B. von Colbe, Y. Zhou, M. Dahms, D.H. Kim, R. Gunther, Y.W. Cho, K.H. Oh, T. Klassen, R. Börmann, M. Dornheim, Acta Mater. 58 3381–3389.
[28] J.J. Vajo, G.L. Olson, Scr. Mater. 56 (2007) 829–834.
[29] E. Deprez, A. Justo, T.C. Rojas, C. López-Cartés, C. Bonatto Minella, U. Bösenberg, M. Dornheim, R. Börmann, A. Fernández, Acta Mater. 58 (2010) 5683–5694.
[30] E. Deprez, M.A. Munoz-Márquez, M.C. Jimenez De Haro, F.J. Palomares, F. Soria, M. Dornheim, R. Börmann, A. Fernández, J. Appl. Phys. 109 (2011) 014913.
[31] E. Deprez, M.A. Munoz-Márquez, M.A. Roldán, C. Prestipino, F.J. Palomares, C.B. Minella, U. Bösenberg, M. Dornheim, R. Börmann, A. Fernández, J. Phys. Chem. C 114 3309–3317.
[32] A. Fernández, E. Deprez, O. Friedrichs, Int. J. Hydrogen Energy 36 (2011) 3932–3940.
[33] S. Garroni, C. Milanese, A. Girella, A. Marini, G. Mulas, E. Menendez, C. Pistidda, M. Dornheim, S. Surinach, M.D. Baró, Int. J. Hydrogen Energy 35 (2010) 5434–5441.
[34] S. Garroni, C. Milanese, D. Pottmaier, G. Mulas, P. Nolis, A. Girella, R. Caputo, D. Olid, F. Teixdor, M. Baricco, A. Marini, S. Surinach, M.D. Baró, J. Phys. Chem. C 115 (2011) 16664–16671.
[35] S. Garroni, C.B. Minella, D. Pottmaier, C. Pistidda, C. Milanese, A. Marini, S. Enzo, G. Mulas, M. Dornheim, M. Baricco, O. Gutfleisch, S. Surinach, M.D. Baró, Int. J. Hydrogen Energy 38 (2013) 2363–2369.
[36] S. Garroni, C. Pistidda, M. Brunelli, G.B.M. Vaughan, S. Surinach, M.D. Baró, Scr. Mater. 60 (2009) 1129–1132.
[37] J.F. Mao, X.B. Yu, Z.P. Guo, H.K. Liu, Z. Wu, J. Ni, J. Alloy. Compd. 479 (2009) 619–623.
[38] C.C. Nwakwuo, C. Pistidda, M. Dornheim, J.L. Hutchison, J.M. Sykes, Int. J. Hydrogen Energy 37 (2012) 2382–2387.
[39] C.C. Nwakwuo, C. Pistidda, M. Dornheim, J.L. Hutchison, J.M. Sykes, Scr. Mater. 64 (2011) 351–354.
[40] C. Pistidda, G. Barkhordarian, A. Rzeszutek, S. Garroni, C.B. Minella, M.D. Baró, P. Nolis, R. Börmann, T. Klassen, M. Dornheim, Scr. Mater. 64 (2011) 1035–1038.
[41] C. Pistidda, S. Garroni, C.B. Minella, F. Dolci, T.R. Jensen, P. Nolis, U. Bösenberg, Y. Cerenius, W. Lohstroh, M. Fichtner, M.D. Baró, R. Börmann, M. Dornheim, J. Phys. Chem. C 114 (2010) 21816–21823.
[42] C. Pistidda, E. Napolitano, D. Pottmaier, M. Dornheim, T. Klassen, M. Baricco, S. Enzo, Int. J. Hydrogen Energy 38 (2013) 10479–10484.
[43] D. Pottmaier, C. Pistidda, E. Groppo, S. Bordiga, G. Spoto, M. Dornheim, M. Baricco, Int. J. Hydrogen Energy 36 (2011) 7891–7896.
[44] C. Pistidda, D. Pottmaier, F. Karimi, S. Garroni, A. Rzeszutek, M. Tolkiehn, M. Fichtner, W. Lohstroh, M. Baricco, T. Klassen, M. Dornheim, Int. J. Hydrogen Energy 39 (2014) 5030–5036.
[45] K.S. Alcantara, J.M. Ramallo-Lopez, U. Bösenberg, I. Saldan, C. Pistidda, F.G. Requejo, T. Jensen, Y. Cerenius, M. Sørby, J. Avila, J.B. von Colbe, K. Taube, T. Klassen, M. Dornheim, J. Phys. Chem. C 116 (2012) 7207–7212.
[46] G. Barkhordarian, T.R. Jensen, S. Doppiu, U. Bösenberg, A. Borgschulte, R. Gremaud, Y. Cerenius, M. Dornheim, T. Klassen, R. Börmann, J. Phys. Chem. C 112 (2008) 2743–2749.
[47] C. Bonatto Minella, S. Garroni, D. Olid, F. Teixidor, C. Pistidda, I. Lindemann, O. Gutfleisch, M.D. Baró, R. Börmann, T. Klassen, M. Dornheim, J. Phys. Chem. C 115 (2011) 18010–18014.
[48] C.B. Minella, C. Pistidda, S. Garroni, P. Nolis, M.D. Baró, O. Gutfleisch, T. Klassen, R. Börmann, M. Dornheim, J. Phys. Chem. C 117 (2013) 3846–3852.
[49] C. Suryanarayana, Prog. Mater. Sci. 46 (2001) 1–184.
[50] K. Zeng, T. Klassen, W. Oelerich, R. Börmann, Int. J. Hydrogen Energy 24 (1999) 989–1004.
[51] B.S. Clausen, G. Steffensen, B. Fabius, J. Villadsen, R. Feidenhansl, H. Topsoe, J. Catal. 132 (1991) 524–535.
[52] J.A. Rodriguez, J.C. Hanson, A.I. Frenkel, J.Y. Kim, M. Perez, J. Am. Chem. Soc. 124 (2002) 346–354.
[53] T.R. Jensen, T.K. Nielsen, Y. Filinchuk, J.-E. Jorgensen, Y. Cerenius, E.M. Gray, C.J. Webb, J. Appl. Crystallogr. 43 (2010) 1456–1463.
[54] http://www.esrf.eu/computing/scientific/FIT2D/.
[55] H. Okamoto, J. Phase Equilib. 14 (1993) 534–535.
[56] Y. Nakamori, G. Kitahara, A. Ninomiya, M. Aoki, T. Noritake, S.I. Towata, S.I. Orimo, Mater. Trans. 46 (2005) 2093–2097.
[57] O.I. Velikokhatnyi, P.N. Kumta, Mater. Sci. Eng. B 140 (2007) 114–122.
[58] D.H. Gregory, J. Mater. Chem. 18 (2008) 2321–2330.
[59] J.J. Vajo, S.L. Skeith, F. Mertens, J. Phys. Chem. B 109 (2005) 3719–3722.
[60] S. Feliu Jr., C. Maffiotte, J.C. Galván, V. Barranco, Corros. Sci. 53 (2011) 1865–1872.
[61] S. Feliu Jr., C. Maffiotte, A. Samaniego, J.C. Galván, V. Barranco, Electrochim. Acta 56 (2011) 4554–4565.
[62] S. Feliu Jr., A. Pardo, M.C. Merino, R. Arrabal, E. Matykina, Adv. Mater. Sci. Eng. (2009) 1–7.
[63] S. Feliu Jr., A. Pardo, M.C. Merino, A.E. Coy, F. Viejo, R. Arrabal, Appl. Surf. Sci. 255 (2009) 4102–4108.
[64] S. Feliu Jr., A. Samaniego, E.A. Bermudez, A.A. El-Hadad, I. Llorente, J.C. Galván, Materials 7 (2014) 2534–2560.
[65] K. Asami, S. Ono, J. Electrochem. Soc. 147 (2000) 1408–1413.
[66] T. Do, S.J. Splinter, C. Chen, N.S. McIntyre, Surf. Sci. 387 (1997) 192–198.
[67] J.C. Fuggle, L.M. Watson, D.J. Fabian, S. Affrossman, Surf. Sci. 49 (1975) 61–76.
[68] N.S. McIntyre, C. Chen, Corros. Sci. 40 (1998) 1697–1709.
[69] M. Santamaria, F. Di Quarto, S. Zanna, P. Marcus, Electrochim. Acta 53 (2007) 1314–1324.
[70] S.J. Splinter, N.S. McIntyre, W.N. Lennard, K. Griffiths, G. Palumbo, Surf. Sci. 292 (1993) 130–144.
[71] A. Andreasen, Int. J. Hydrogen Energy 33 (2008) 7489–7497.
[72] S. Bouaricha, J.P. Dodelet, D. Guay, J. Huot, S. Boily, R. Schulz, J. Alloy. Compd. 297 (2000) 282–293.
[73] J.C. Crivello, T. Nobuki, S. Kato, M. Abe, T. Kuji, J. Alloy. Compd. 446–447 (2007) 157–161.
[74] J.C. Crivello, T. Nobuki, T. Kuji, Int. J. Hydrogen Energy 34 (2009) 1937–1943.
[75] M. Sato, T. Kuji, Mater. Trans. 52 (2011) 1773–1776.
[76] S. Couillaud, E. Gaudin, F. Weill, S. Gomez, C. Stan, D. Plante, S. Miraglia, J.L. Bobet, Acta Mater. 60 (2012) 4144–4151.
[77] J.L. Bobet, B. Chevalier, M.Y. Song, B. Darriet, J. Etourneau, J. Alloy. Compd. 336 (2002) 292–296.
[78] Z. Li, X. Liu, L. Jiang, S. Wang, Int. J. Hydrogen Energy 32 (2007) 1869–1874.
[79] S. Orimo, H. Fujii, M. Tabata, J. Alloy. Compd. 210 (1994) 37–43.
[80] H.Y. Leng, T. Ichikawa, S. Hino, N. Hanada, S. Isobe, H. Fujii, J. Power Sources 156 (2006) 166–170.
[81] F.W. Bergstrom, W.C. Fernelius, Chem. Rev. 12 (1933) 43–179.